Universal transport properties of three-dimensional topological insulator nanowires

Lei Zhang,[1,2] Jianing Zhuang,[1] Yanxia Xing,[3] Jian Li,[4] Jian Wang,[1,*] and Hong Guo[2]

[1]*Department of Physics and the Center of Theoretical and Computational Physics, The University of Hong Kong, Hong Kong, China*

[2]*Department of Physics, McGill University, Montreal, Canada*

[3]*Department of Physics, Beijing Institute of Technology, Beijing 100081, China*

[4]*Department of Physics, The University of Geneva, Geneva, Switzerland*

(Received 26 March 2013; revised manuscript received 29 January 2014; published 6 June 2014)

We report theoretical calculations of electronic and transport properties mediated by topological helical states on the *walls* of three-dimensional topological insulator (TI) *nanowires*. A universal regime of quantized conductance and fluctuations is found that is induced by disorder. The average conductance of the disordered nanowire scales as a function of the number of transmission channels N in a universal form $\langle G\rangle = \alpha N + \beta$, independent of the system details. For instance, for Bi_2Se_3 nanowires cleaved along the x or y direction with the quintuple layers along the z direction, $\langle G_{xx}\rangle = (5/12)N + 1/2$. The universal and quantized behavior is due to the topological physics happening on the walls of the nanowire under the influence of disorder.

DOI: 10.1103/PhysRevB.89.245107 PACS number(s): 73.23.−b, 62.23.Hj, 72.10.Fk, 73.25.+i

I. INTRODUCTION

The notion of a topological insulator (TI) [1–3] has attracted great attention due to its fundamental role in classifying electronic structures of materials having a band gap. On the surface of TI there are conducting helical states induced by the spin-orbit interaction (SOI) and protected by time-reversal symmetry [4]. A peculiar property of helical states is that their direction of electron spin is locked to perpendicular to the electron momentum $\mathbf{k}$, as such back scattering ($\mathbf{k} \to -\mathbf{k}$) by disorder is suppressed because the electron's spin cannot be flipped if the disorder does not break time-reversal symmetry. A multitude of applications of TI materials have been envisioned [3] based on this peculiar property. A prototypical material of three-dimensional (3D) TI is the Be_2Se_3 compound [5], which has a layered structure consisting of repeated quintuple layers of atoms extending along, say, the z direction. Each quintuple contains five atomic layers of the Be and Se atoms, the quintuples are held together by van der Waals forces to form the bulk crystal. Thin films of TI have been grown and helical states on the two surfaces of the film were the subject of extensive investigations.

More recently, *nanowires* of TI were fabricated [6] and these mesoscopic structures posed very interesting questions concerning the properties of helical states on the wall surfaces of the *nanowire*. For instance, a square-shaped nanowire has four side-walls, what kind of helical states exist on these walls, how do they distribute spatially and couple to each other? What are the transport properties of the nanowires under the influence of static disorder? It is the purpose of this paper to report systematic theoretical investigations of helical states of TI *nanowires*.

It turns out that helical states on the walls of a TI nanowire have their own very peculiar properties which manifest in the behavior of conductance and its fluctuations. For a wide range of disorder parameters, the average conductance of the TI wires obeys $\langle G\rangle = \alpha N + \beta$, where N is the number of transmission channels of the helical states and α, β are *universal* and *fractional* constants independent of the details of the system, but depending on which crystalline direction the nanowire is cleaved. As a result, $\langle G\rangle$ is *fractionally quantized* in a universal way over the energy gap of the TI and over large disorder parameters, while at the same time the conductance fluctuation is also *quantized*. Fractionally quantized conductance is, of course, intriguing and our investigation found it is due to the interplay between the topological surface states on the walls of the *nanowire* and the effects of disorder.

Note that disorder-induced *integer quantization* in two and three dimensions of the proposed topological Anderson insulator was theoretically contemplated [7–10] where disorder destroys bulk states to reveal the surface states leading up to conductance $G = 2$ in units of conductance quanta. In addition, the *fractional quantization* of G due to a strong electron-electron interaction was also theoretically proposed [11–15], reminiscent of the fractional quantum Hall effect. In all these situations, G is completely determined by the topological states and has no accompanied fluctuation. On the other hand, the fractional quantization in TI nanowires which we report is a different mesoscopic topological phenomenon in which both the average G and its fluctuation take quantized universal values. The physical origin of this phenomenon will be identified.

II. THEORETICAL MODEL

We consider two kinds of nanowires. The first is cleaved to extend along the x or y direction for which two of the four walls expose the quintuple surface, as shown in Fig. 1(a). The second is cleaved to extend along the z direction for which none of the four walls expose the quintuple surface, as shown in Fig. 1(b). The nanowire is in contact with source/drain electrodes to form a two-terminal device. The electronic structure of the Be_2Se_3 material near the Dirac point can be described by the following effective Hamiltonian $H(\mathbf{k})$ matrix [16]:

$$H(\mathbf{k}) = \epsilon_0(\mathbf{k})\mathbf{I} + \begin{bmatrix} M(\mathbf{k}) & A_1 k_z & 0 & A_2 k_- \\ A_1 k_z & -M(\mathbf{k}) & A_2 k_- & 0 \\ 0 & A_2 k_+ & M(\mathbf{k}) & -A_1 k_z \\ A_2 k_+ & 0 & -A_1 k_z & -M(\mathbf{k}) \end{bmatrix}, \quad (1)$$

*jianwang@hku.hk

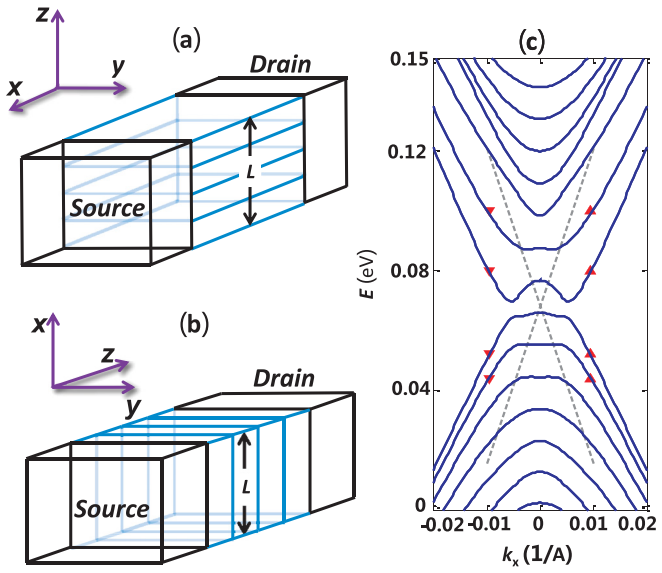

FIG. 1. (Color online) Square-shaped Bi_2Se_3 nanowires contacted by source/drain electrodes. The normal of the quintuples of Bi_2Se_3 is along the z axis. (a) Transport along the x direction, the top and bottom walls expose the quintuple surface. (b) Transport along the z direction, none of the walls expose the quintuple surface. (c) The calculated band structure for the wire of (a). The red symbols indicate energies and k points where the local density of states (LDOS) are shown in Fig. 2 below. The two dashed lines are schematic of the Dirac bands of bulk TI.

where $\mathbf{I}$ is a 4×4 identity matrix; $k_\pm \equiv k_x \pm ik_y$; $M(\mathbf{k}) = M - B_1k_z^2 - B_2(k_x^2+k_y^2)$; and $\epsilon_0(\mathbf{k}) = C + D_1k_z^2 + D_2(k_x^2 + k_y^2)$. To investigate the nanowires of Fig. 1, the Hamiltonian is discretized on a cubic mesh with $k_\alpha = -i\frac{\partial}{\partial\alpha}$ where $\alpha = x,y,z$. We consider the effects of static Anderson-type disorder to the on-site energy with a uniform distribution in the interval $[-W/2,W/2]$, where the parameter $|W/2|$ gives the largest possible disorder strength of any site. The average strength of the disorder is denoted by $\Delta \equiv W/4$, which gives the measure of disorder strength. In the Hamiltonian, parameters $A_1,A_2,B_1,B_2,C,D_1,D_2$, and M characterize the Be_2Se_3 material which was obtained by fitting to experiments and/or to first-principles calculations, taken from Ref. [16]. From the Hamiltonian, we numerically solve the electronic and transport properties of the two-terminal nanowire device.

For *bulk* TI, the Hamiltonian Eq. (1) produces two Dirac linear bands induced by the spin-orbit interaction, as schematically shown by the dashed lines in Fig. 1(c). For *nanowires*, these Dirac bands split into many subbands due to the transverse finite-size confinement, as shown by the curves in Fig. 1(c) for a wire cleaved along x [Fig. 1(a)]. Each subband corresponds to two time-reversal degenerate transmission channels. A small pseudogap also develops at the Dirac point due to confinement. Quantum transport is mediated by these subbands, which correspond to helical states on the walls of the wire.

A. Nanowire without disorder

Before analyzing quantum transport in disordered nanowires, let us understand the electronic states of pristine wires. A very interesting result is that for the wire with walls exposing the quintuple surface [Fig. 1(a)], helical states are always confined on *opposite* walls of the wire, i.e., they become *stripe states*. We shall call them a type-I helical state. On the other hand, for wires with no quintuple surface walls [Fig. 1(b)], the helical states always extend over the *adjacent* walls or over all four walls. We call these type-II helical states.

The type-I helical state and its spin texture are schematically shown in Figs. 2(a) and 2(b) whose spatial distribution is vividly displayed by plotting the local density of states (LDOS) on the transverse cross section. Picking several energies $E = 0.043$ to 0.098 (in units of eV) at fixed $|k| = 0.01$, the LDOS are shown in Figs. 2(c) to 2(f) showing that the type-I helical states locate at opposite walls of the wire. We found this is true for all energies near the Dirac point [17]. The results thus indicate that when nanowires are cleaved to extend along the x (or y) direction, the helical states are completely separated by localizing on opposite walls. Such a spatial separation strongly suppresses back scattering by minimizing the interactions between the states. The localization on *opposite* walls is due to a strong anisotropy along the y and z directions when the wire is cleaved along x because for Bi_2Se_3, the parameters $D_2 \gg D_1$ and $B_2 \gg B_1$ in the Hamiltonian Eq. (1). Which pair of walls does the type-I helical states locate? We found it is localized to the x-z plane [Figs. 2(a), 2(c), and 2(d)] when energy is below the Dirac point; and to the x-y plane [Figs. 2(b), (e), and (f)] when the energy is above. This property can be understood by projecting the 3D Hamiltonian Eq. (1) onto the x-z and x-y planes [16,18] and the reduced model shows that it is the anisotropy that is responsible for the location of the states. More details about this analysis can be found in the Appendix.

The calculated type-II helical state and its spin texture—on the walls of the nanowire cleaved along the z direction [Fig. 1(b)—is schematically shown in Fig. 2(g). Figures 2(h) and 2(i) are the LDOS at energy $E = 0.068$ where there are two transmission channels. One helical state is centered at the lower-left corner [Fig. 2(h)] and the other at the upper-right corner [Fig. 2(i)], both extending to the adjacent walls.

The conductance G of an infinitely long pristine nanowire is determined by the number of transmission channels N at any given energy E, namely $G(E) = N(E)$ in units of conductance quanta e^2/h. The integer N can be directly read off from the band structure of the pristine wire at any given energy E. In the following we show that when there is disorder in the nanowires, the average G can be universally and *fractionally* quantized.

B. Nanowire with disorder

In the presence of disorder, we perform transport calculations by discretizing the wire on a $L\times L\times L(a^3)$ mesh with mesh size $a = 10$ Å [19]. As mentioned above, Anderson-type disorder is applied that is characterized by the parameter Δ. In addition to the two-terminal devices shown in Figs. 1(a) and 1(b), we also investigated another device where the source and drain electrodes are perpendicular to each other. The two-terminal structures are schematically shown as the insets in Figs. 3(a) 3(c), and 3(e). Hence there are four relevant conductances G_{zz}, $G_{xx} = G_{yy}$, G_{xy} and G_{zx}, where

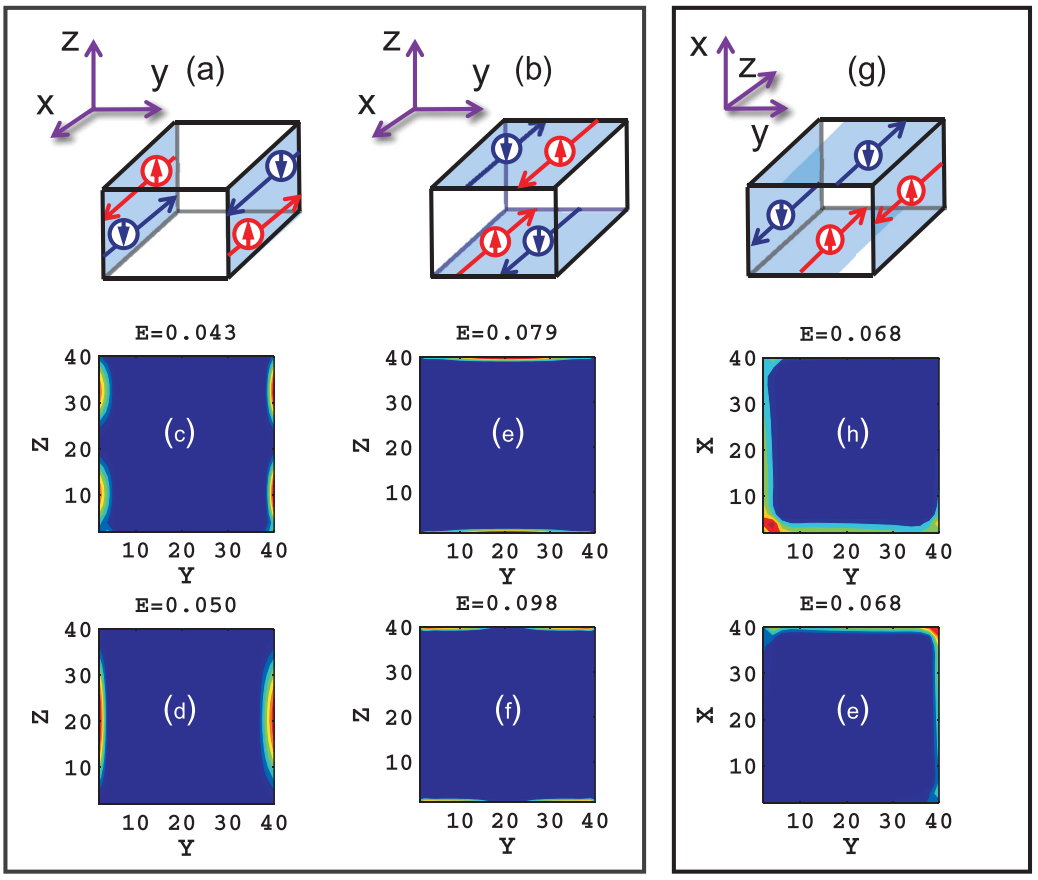

FIG. 2. (Color online) Calculated real-space LDOS on a transverse cross section of the wire, plotted on a 40×40 mesh with mesh-spacing 10 Å. The box on the left is for type-I helical states, which are always located on *opposite* walls of the wire; the box on the right is for type-II states, which are always located on the *adjacent* walls of the wire. Due to time-reversal symmetry, the helical states come in pairs. (a, b, g) are schematics of the calculated helical states and their spin textures. (c, d, e, f) are LDOS of type-I helical states at four different energies; (h, i) are LDOS of type-II at a same energy.

the subscripts ij mean electrons incoming from the j direction and outgoing to the i direction.

Figure 3 plots the average conductance $\langle G\rangle$ and the root-mean square (rms) rms(G) for nanowires with $L = 20\,(N = 2)$ versus the disorder parameter Δ, at the energy inside the bulk gap so that only topological states contribute to conduction. At very weak Δ, we obtain $\langle G\rangle = 2$ and rms(G) ≈ 0 as expected. Increasing Δ causes $\langle G\rangle$ to gradually reduce while rms(G) gradually increases, but incredibly, at a moderate but wide range of Δ when the system is in the diffusive regime, both $\langle G\rangle$ and rms(G) become *quantized*. In fact, the quantized $\langle G\rangle$ and rms(G) are also *universal* because it is independent of material parameters (see below). As shown in Fig. 3, the quantized $\langle G\rangle$ takes *fractional* values, $\langle G_{zz}\rangle = 1$, $\langle G_{xx}\rangle = \langle G_{yy}\rangle = 4/3$, and $\langle G_{zx}\rangle = 6/5$, independent of Δ for a wide range up to $\Delta = 1$ eV.

We have carried out calculations for disordered nanowires with much larger cross sections and thus more subbands, e.g., for $L = 40$ and 60, which have three ($N = 6$) and five subbands ($N = 10$), respectively. By sweeping through the electron energy E for the $L = 60$ nanowire, five quantized $\langle G\rangle$'s with fractional values were obtained corresponding to the five different subbands. For the type-I and type-II helical states characterized by the conductance G_{xx} and G_{zz}, the results have an excellent linear scaling on N, which is very accurately consistent with $\langle G_{xx}\rangle = (5/12)N + 1/2$ and $\langle G_{zz}\rangle = (3/10)N + 2/5$ for $N > 0$. Clearly, for the $L = 20$ nanowires having $N = 2$, this reduces to $\langle G_{xx}\rangle = 4/3$; precisely the value shown in Fig. 3(c). In addition, for the nanowires with $L = 40$, the calculated $\langle G_{xx}\rangle$ data all fall precisely on this scaling expression. We summarize further details of the numerical computation in the Appendix.

Why can $\langle G\rangle$ of the TI nanowires be *quantized* for a wide range of Δ values in the diffusive regime? This is qualitatively understood by considering how disorder affects the helical states on the walls of the nanowire. As shown in Fig. 2, for clean samples the type-I helical states are localized on the opposite walls while the type-II states are localized on the adjacent walls. These topological states are protected by the time-reversal symmetry; thus small Δ could not derail them. By increasing Δ, helical states localized on the opposite walls start to spread over to the adjacent walls and the coupling between the forward-moving (FM) and backward-moving (BM) helical states [see Figs. 2(a), 2(b), and 2(c)] increases, $\langle G\rangle$ is therefore reduced, e.g., going down from $\langle G\rangle = 2$ continuously as shown in Figs. 3(a) and 3(c). Increase Δ further and eventually the FM and BM helical states are coupled to the maximum possible extent so that $\langle G\rangle$ cannot be decreased further by Δ, thus a quantized plateau versus Δ is obtained. The quantized plateau persists until such a large Δ

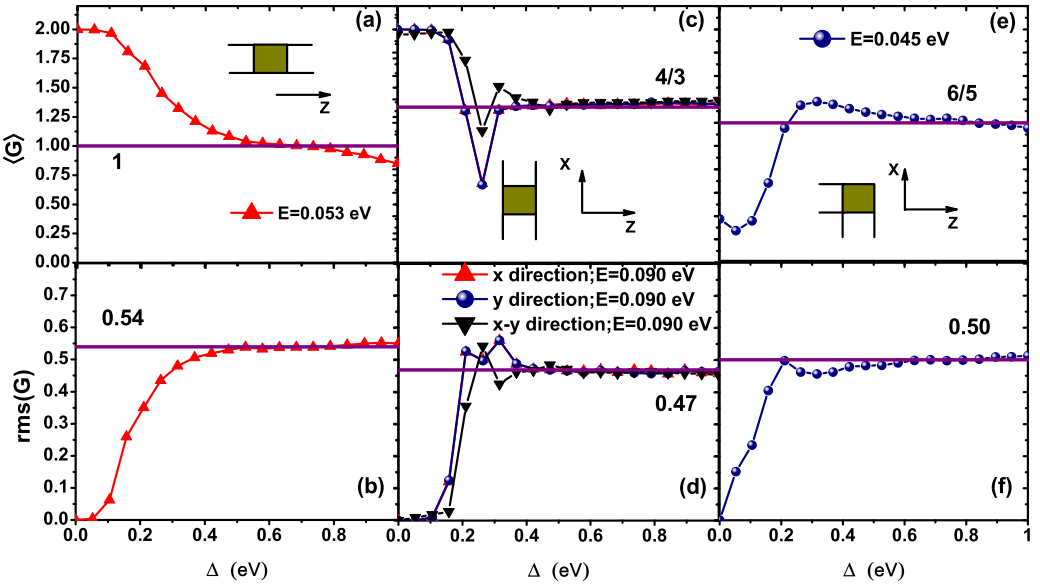

FIG. 3. (Color online) Average conductance and its fluctuation versus parameter Δ for different transport directions: (a, b) G_{zz}; (c, d) G_{xx}, G_{yy}, and G_{xy}; and (e, f) G_{xz}. Each data point on the figure is averaged over 5000 disorder configurations.

when the helical states not only spread over the four walls of the wire but also penetrate into the interior of it. At that point, $\langle G\rangle$ starts to reduce again as can be decerned at the large Δ end in Figs. 3(a), 3(c), and 3(e).

To substantiate the above physical picture, we calculated the LDOS of type-I helical states by averaging different configurations with $\Delta = 0.19$ and 0.32 (see Fig. 4). $\Delta = 0.19$ is at the first drop of $\langle G\rangle$ in Fig. 3(b) while $\Delta = 0.32$ is at the quantized plateau. The spreading of the helical states around the walls of the nanowire is evident. For $\Delta = 0.32$ and other values on the plateau, some LDOS has penetrated to the interior of the wire but has not percolated into a conduction pathway, hence the quantization is maintained. We conclude that the quantized regime of $\langle G\rangle$ is due to the topological physics happening on the walls of the nanowires where the forward and backward moving helical states reach a maximum mixing by the disorder. It is indeed extremely interesting to obtain that the quantized value of $\langle G\rangle$ happens to be *fractional*. It is also very interesting that rms(G) is a constant in the same range of Δ, reminiscent of the universal conductance fluctuation of mesoscopic metal wires [20]. Note that if one considers the overlap of FM and BM helical states on the walls of nanowires with disorder, the localization physics will eventually play a role at large Δ and for very long wires beyond the localization length [21].

In the following we use the phenomenological theory of mode mixing [22] to account for the numerical data, using $N = 2$ incoming channels. Let us define *effective transmission channel* number ν_t and *reflection channel* number ν_r. In the diffusive regime it is reasonable to assume that the two incoming channels are evenly distributed among the effective transmission and reflection channels after scattering.

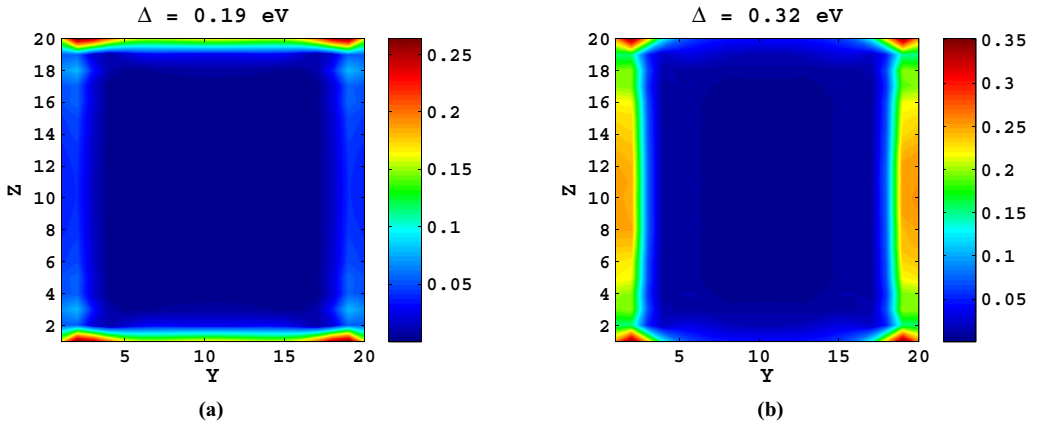

FIG. 4. (Color online) Calculated real-space LDOS on the middle transverse cross section of the wire in Fig. 3(c), plotted on a 20 × 20 mesh with mesh spacing 10 Å, for two values of Δ. (a) $\Delta = 0.19$, which is at the first downturn of $\langle G\rangle$ in Fig. 3(c), showing that the type-I helical states on the opposite walls (top and bottom) start to couple by going around the walls. (b) $\Delta = 0.32$, which is at the beginning of the quantized region in Figs. 3(c) and 3(d), showing that type-I helical states are now well coupled and going around all four walls of the wire.

In terms of (ν_r,ν_f), the conductance is given by the following expression:

$$\langle G\rangle = 2\nu_t\nu_r/(\nu_t+\nu_r), \tag{2}$$

where we identify the parameters to be $(\nu_r,\nu_t) = (1,1)$, $(1,2)$, and $(1,1.5)$ for G_{zz}, G_{xx}, and G_{zx}, respectively (see details in the Appendix). These (ν_r,ν_t) values reproduce the average conductance presented above. For the universal conductance fluctuations, we propose the following expression:

$$\mathrm{rms}(G) = 2\langle G\rangle/\sqrt{4(\nu_t+\nu_r)^2-2}. \tag{3}$$

With the same set of (ν_r,ν_f) we find from Eq. (3) that $\mathrm{rms}(G_{zz}) = 0.535$, $\mathrm{rms}(G_{xx}) = 0.457$, and $\mathrm{rms}(G_{zx}) = 0.500$ are very close to the numerical results (see Fig. 3).

How robust are the qualitative and quantitative physics? To this end we carried out calculations for nanowires made of a different 3D TI material Sb_2Te_3 [23] having $L = 20$ which has $N = 2$ incoming channels. Exactly the same quantized values of $\langle G\rangle$ and $\mathrm{rms}(G)$ corresponding to G_{xx} and G_{zz} of Fig. 3 are obtained. We also calculated $\langle G\rangle$ and $\mathrm{rms}(G)$ in the presence of "surface" disorder [24,25] in which Δ is added to a few outer layers of the Bi_2Se_3 nanowire. Again, $\langle G_{zz}\rangle$ and $\mathrm{rms}(G_{zz})$ have exactly the same quantized plateau as that of Figs. 3(a) and 3(b). Since the quantization exists for a large range of disorder parameter, for the entire bulk gap of the TI, for two different TI materials, for wires cleaved along different directions, and for surface or bulk disorder models, the disorder-induced quantization of $\langle G\rangle$ and $\mathrm{rms}(G)$ is strongly evidenced to be a piece of universal physics. Finally, the universal quantization is summarized by a calculated phase diagram in the (Δ,E) plane (see the Appendix). The mixing of FM and BM helical states is demonstrated in Fig. 4. Note that if one considers the overlap of forward-moving and backward-moving helical states on the walls of nanowires with disorder, the localization physics will eventually play a role at large Δ and for very long wires beyond the localization length.

Concerning possible experimental verification of our result, we note that the starting point of the universal regime of quantized conductance and fluctuations is found to be $\Delta \sim 310$ meV, which can be accessible experimentally. For instance, in recent experiments copper atoms in the Bi_2Se_3 were doped to form a $Cu_xBi_2Se_3$ alloy which changed the band bending up to hundreds of meV (see Ref. [27]). According to the experiment, they predicted that the band bending by doping copper can be as large as 250 meV. In addition, from the materials point of view, native point defects are often formed in Bi_2Se_3 such as the triangular and topographic features, as well as the Bi_{Se} antisite defects. To summarize, the parameter range of this universal physics should be experimentally accessible in the near future by doping the native TI with impurity atoms, perhaps as in the above experiment.

III. SUMMARY

We report a disorder-induced universal quantization of the conductance and its fluctuation in mesoscopic TI nanowires, which is due to the topological physics happening on the walls of the nanowire. An increasing disorder first spread the helical states over the walls of the nanowire causing a reduction of the average conductance. After the forward- and backward-moving helical states are well coupled, further increasing disorder can no longer can reduce conductance until disorder becomes so strong that the helical states penetrate the interior of the wire. As a result, the average conductance enters a plateau that excellently scales as $\langle G\rangle = \alpha N + \beta$ for all the mesoscopic nanowires, materials, disorder parameter, energy, and other system parameters. For the Bi_2Se_3 wires cleaved along the x (or y) direction, $\langle G_{xx}\rangle = (5/12)N + 1/2$ independent of the system details. Importantly, the conductance fluctuation $\mathrm{rms}(G)$ is also quantized on the same plateau. The predictions and the physical picture should be experimentally testable.

ACKNOWLEDGMENTS

This work was financially supported by RGC (HKU 705611P) and UGC (Contract No. AoE/P-04/08) of the Government of HKSAR. Y.X. is supported by the NSF-China under Grant No. 11174032. J.L. is supported by the Swiss National Center of Competence in Research on Quantum Science and Technology.

APPENDIX

In this Appendix, we present a detailed analysis on five points of the main text. Appendix 1 discusses the physical reason on the location of the type-I helical states (the strip states). By projecting the 3D Hamiltonian Eq. (1) of the main text onto the x-z and x-y planes similar to the approach in Refs. [16,18], the reduced two-band model shows that it is the anisotropy that is responsible to the location of the stripe states. Appendix 2 presents further numerical details for disordered TI nanowires with a larger cross section, thus more subbands, up to $L = 60$ which has five subbands with ten transmission channels ($N = 10$). In Appendix 3, we propose a phenomenological mode-mixing theory to account for the quantized average conductance and its fluctuation plateau. Appendix 4 provides further evidence of the universal quantized conductance and fluctuation in the diffusive regime as well as the discussion on localization length. Finally in Appendix 5, we provide some technical details on the calculation of conductance and its fluctuation.

1. Two-band model

The calculated type-I helical state and its spin texture are schematically shown in Figs. 2(a) and 2(b) of the paper whose spatial distribution is vividly displayed by plotting the LDOS on the transverse cross section as seen in Figs. 2(c) to 2(f). We found that the type-I helical states locate at opposite walls of the wire: they are localized to the x-z plane [Figs. 2(a), 2(c), and 2(d)] when energy is below the Dirac point; and to the x-y plane [Figs. 2(b), 2(e), and 2(f)] when energy is above. This peculiar property can be understood by projecting the 3D Hamiltonian Eq. (1) of the paper to simpler reduced models that can be solved analytically.

Let us begin by a simple one-dimensional (1D) reduction of the model Hamiltonian Eq. (1) of the paper, namely $H \sim [D_1 + (D_2 - D_1)\theta(x)]k^2$ where the kinetic energy is different for an electron at $x < 0$ or $x > 0$. For this one-band model, the transmission amplitude of the electrons is derived as $t =$

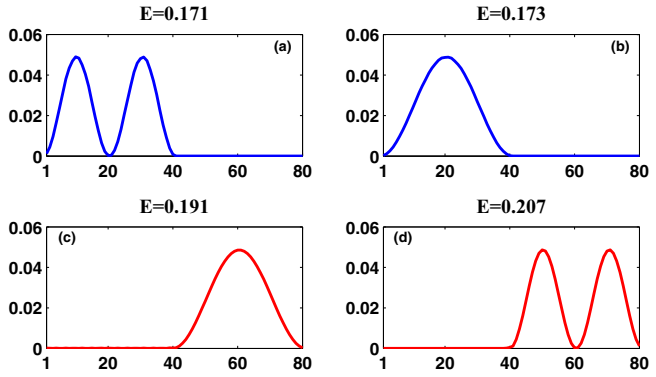

FIG. 5. (Color online) The LDOS of type-I helical states (stripe state) of the two-band model at different energies. Here we have $L = 80$ where the first 40 lattice sites corresponds to the region of the x-z surface and the other region is for the x-y surface.

$2/(1+\kappa)$ where $\kappa^2 = D_2/D_1$. Hence at large anisotropy κ, $|t|^2$ is very small, which means the electrons prefer to stay in the region with small kinetic energy. While this simple argument can only account for the effect of anisotropy below the Dirac point, a full picture for both below and above the Dirac point can be similarly established from a two-band model obtained by projecting the Hamiltonian Eq. (1) onto the x-z and x-y planes.

The projection of Hamiltonian Eq. (1) of the main paper onto the x-z and x-y planes is done similarly to the approach in Refs. [16,18]. The effective Hamiltonian in the x-z and x-y planes are, respectively, given by

$$H^{xz}(k_z) = \alpha_2 + \gamma_2 k_z^2 I_{2\times 2} + \beta_2(A_1\sigma_x k_z - A_2\sigma_z k_x), \quad \text{(A1)}$$

and

$$H^{xy}(k_y) = \alpha_1 + \gamma_1\left(k_x^2 + k_y^2\right) I_{2\times 2} + A_2\beta_1(\sigma_x k_y - \sigma_y k_x), \quad \text{(A2)}$$

where $\alpha_i = C + D_i M/B_i$, $\beta_i^2 = 1 - (D_i/B_i)^2$, $\gamma_1 = D_2 - B_2 D_1/B_1$, and $\gamma_2 = D_1 - B_1 D_2/B_2$. Here $A_1, A_2, B_1, B_2, C, D_1, D_2$, and M are system parameters defined in Ref. [16]. Since we are interested in LDOS on the y-z plane, k_x is a good quantum number; thus H^{xz} and H^{xy} above reduce to one-dimensional two-band models.

Next, consider the two-band Hamiltonian $H \to H^{xz}(k_z = k)$ when $-L/2 < x < 0$, and $H \to H^{xy}(k_y = k)$ when $L/2 > x > 0$. This two-band model can be solved exactly. The solutions of the LDOS at four different energies are shown in Fig. 5. It is evident that the electron localizes in different regions for different energies. The two-band model thus captures the qualitative feature of the type-I helical states shown in Fig. 1, and this analysis shows that it is the anisotropy that is responsible to the location of the stripe states.

2. Average conductance versus N

In this section we present further numerical details for disordered TI nanowires with a larger cross section, thus more subbands, up to $L = 60$ and five subbands corresponding to ten transmission channels ($N = 10$). We calculate $\langle G_{xx}\rangle$ for a $L \times L \times L$ cubic sample with $L = 60$ and a mesh size of 10 Å. As the electron energy E is increased, more transmission

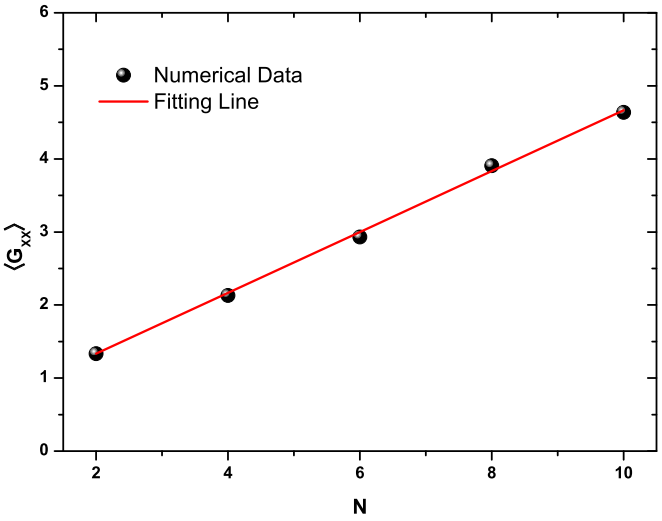

FIG. 6. (Color online) The average conductance $\langle G_{xx}\rangle$ versus number of transmission channels N, for wires having $L = 60$. Three thousand disorder configurations are calculated and averaged for each data point. The data points very accurately fit $\langle G_{xx}\rangle = (5/12)N + 1/2$, shown by the red line.

channels N become available. The $\langle G_{xx}\rangle$ as a function of N is calculated for N up to 10. The result is shown in Fig. 6 where we have fixed the disorder parameter $\Delta = 0.5$ eV so that the system is in the diffusive regime. From Fig. 6, $\langle G_{xx}\rangle$ scales linearly with N. The linear fit very precisely scales as $\langle G_{xx}\rangle = (5/12)N + 1/2$ for $N > 0$. We have also calculated the average conductance $\langle G_{zz}\rangle$ right at the plateau region and it scales as $\langle G_{zz}\rangle = (3/10)N + 2/5$ for $N > 0$.

To confirm that these scaling laws hold for other wires (different L), in Fig. 7 we plot the calculated $\langle G_{zz}\rangle$, $\langle G_{xx}\rangle$ [Figs. 7(a) and 7(c)] and their fluctuations [Figs. 7(b) and 7(d)] as a function of Δ for wires with $L = 30$ where there are four incoming transmission channels ($N = 4$). We see that the plateau values of $\langle G_{zz}\rangle$ and $\langle G_{xx}\rangle$ obey the scaling relation very well. Figure 8 plots $\langle G_{zz}\rangle$, $\langle G_{xx}\rangle$ [Figs. 8(a) and 8(c)] and their fluctuations [Figs. 8(b) and 8(d)] as a function of Δ for $L = 40$ wires which has $N = 6$. Again, the results obey the same scaling laws.

We conclude that the results are independent of many system details as discussed in the main text of the paper, suggesting that the fractional average conductance is a generic feature of the helical states on the walls of TI nanowires in the presence of disorder.

3. Mode mixing theory for quantized conductance and its fluctuations

In this section, we propose a phenomenological mode-mixing theory to account for (and organize) our numerical results, using the case of $N = 2$. The original mode-mixing theory was used to explain the observed fractional quantization of conductance of the quantum Hall effect in disordered graphene [26]. According to this theory [22], the incoming channels are uniformly distributed among the outgoing channels (e.g., transmission and reflection) in the diffusive regime. We refer to this situation as "complete mixing." For conductance G_{zz} with $N = 2$, complete mixing means that the two incoming channels uniformly distribute on four outgoing

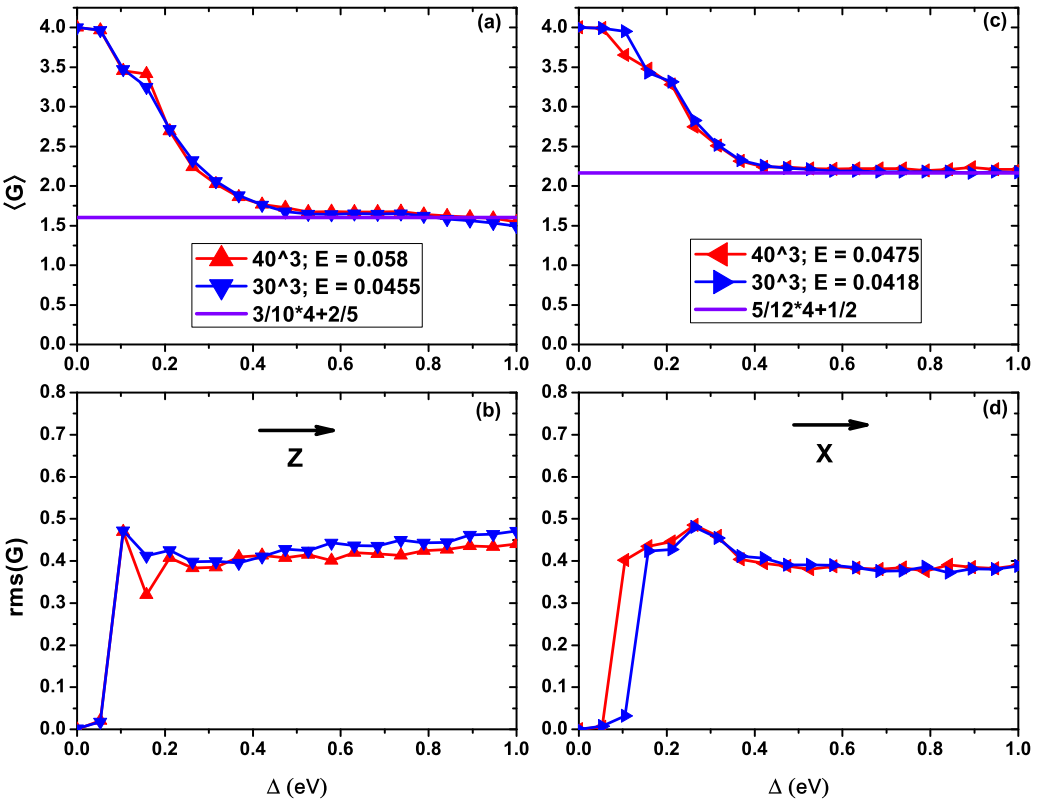

FIG. 7. (Color online) Average conductance ($N = 4$) and its root mean square (fluctuation) value versus disorder strength Δ for wires having $L = 30$ (blue curve) and $L = 40$ (red curve) and for different transport directions: (a, b) G_{zz} and (c, d) G_{xx}. Each data point on the figure is averaged over 1500 disorder configurations.

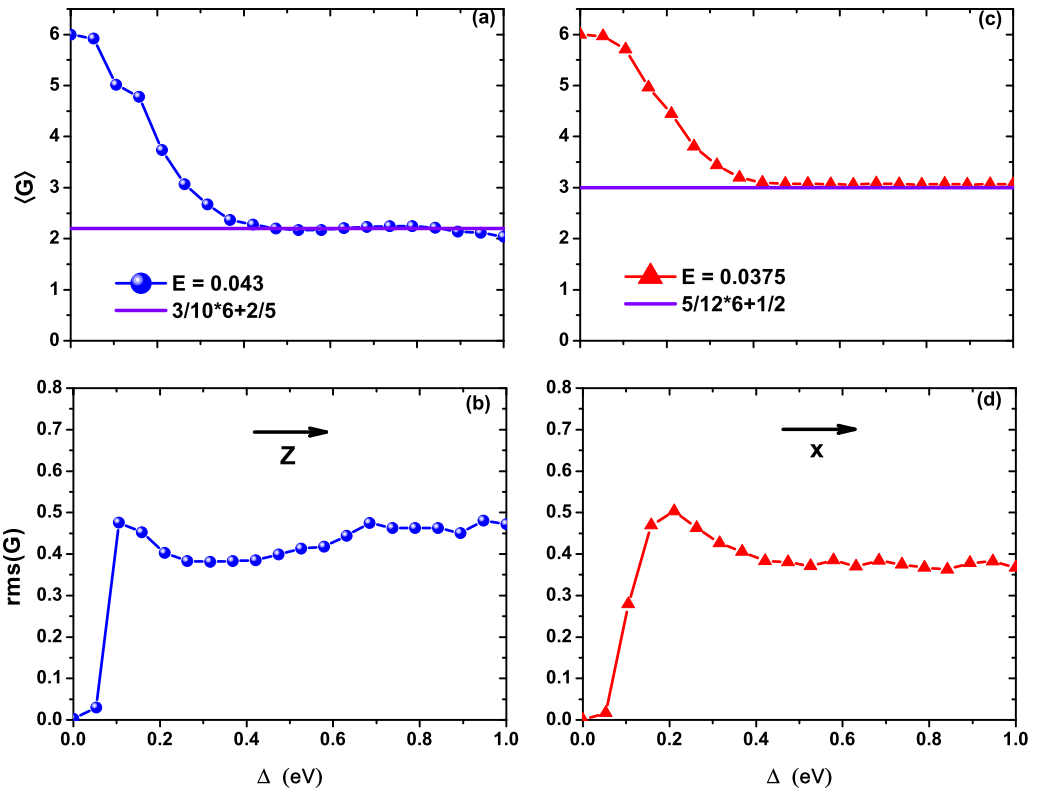

FIG. 8. (Color online) Average conductance ($N = 6$) and its root mean square (fluctuation) value versus disorder strength Δ for different transport directions: (a,b) G_{zz} and (c, d) G_{xx}. Each data point on the figure is averaged over 1500 disorder configurations.

channels (two for reflection and two for transmission), giving rise to the quantized conductance $G_{zz} = 1$, which agrees with our numerical data.

For the conductance G_{xx} and G_{xz}, however, complete mode mixing does not apply due to the strong anisotropy in the y and z directions. We propose a "partial mode mixing" where the two incoming channels are *unevenly* distributed among the four outgoing channels. To describe the distribution among outgoing channels we can use the probability p_t and p_r for transmission and reflection, respectively. If it is evenly distributed, $p_t = p_r = 1/2$; if it is unevenly distributed p_t and p_r are not equal.

Alternatively, we can introduce phenomenological parameters "effective transmission channels" and "effective reflection channels" so that the complete mode mixing can be used again. In other words, instead of two reflection and two transmission channels, the "effective outgoing channels" are ν_r for reflection and ν_t for transmission, satisfying $\nu_t/\nu_r = p_t/p_r$. Now we have $\nu_r + \nu_t$ effective outgoing channels instead of four outgoing channels. Applying the complete mode-mixing picture (i.e., the two incoming channels are evenly distributed on $\nu_r + \nu_t$ outgoing channels), one naturally obtains Eq. (2) of the main text for the average conductance. Furthermore, we proposed a formula Eq. (3) in the main text for the conductance fluctuation where the only inputs are parameters ν_r and ν_t. As we see from the main text, the proposed formula reproduces very well the conductance fluctuation for three cases, rms(G_{zz}), rms(G_{xx}), and rms(G_{xz}). We wish to point out that Eq. (2) in the main text is different from Eq. (4) in Ref. [22].

We conclude that all our numerical data can be accounted for by the phenomenological mode-mixing theory. In the diffusive regime, incoming electrons are randomly scattered elastically to make the mode-mixing idea reasonable. Nevertheless, further investigation is perhaps needed to elucidate why this phenomenological idea works so well for disordered TI nanowires.

4. Phase diagram of quantized conductance G_{zz}

To demonstrate the universal feature of the quantized conductance and its fluctuation, we have calculated the phase diagram where $\langle G_{zz}\rangle$ and rms(G_{zz}) are plotted in the (Δ,E) plane, as shown in Fig. 9. In the calculation, the periodic condition in the x direction is employed. The large light green area ($\Delta \sim [0.38, 1.25]$ for $E = 0.05$) is the found quantization region. For the entire range of E (inside the bulk gap), transport evolves from the behavior of a pristine topological insulator (for which $G = 2$) to the region of disorder-induced quantization of $\langle G\rangle$ (light green). As Δ increases to very large values beyond 1.5 eV, transport evolves to the localized regime and eventually $\langle G\rangle \approx 0$. The phase diagram shows that there is a large phase space in the (Δ,E) plane where conductance and its fluctuation are independent of electron energy and disorder strength.

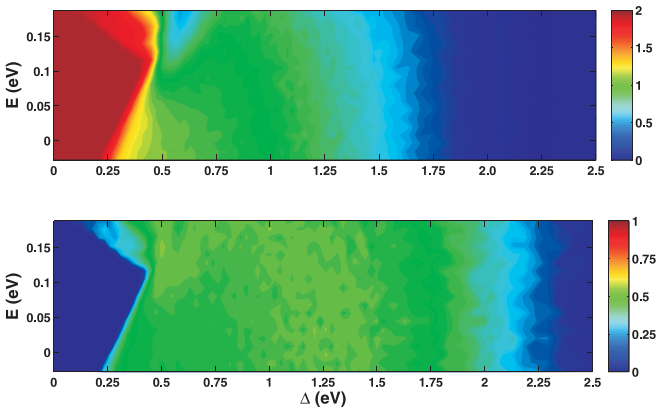

FIG. 9. (Color online) Calculated "phase diagram" in the (Δ,E) plane for nanowire of Fig. 1(b) in the main text. The large light green area is the found quantization region for $\langle G_{zz}\rangle$ (upper panel) and rms(G_{zz}) (lower panel). One thousand nanowire samples are calculated and averaged for each point on this phase diagram.

5. Technical details on calculation of conductance and its fluctuation

By using Green's functions, we calculate the charge conductance from the terminal L to the terminal R using the Landauer-Büttiker formula $G(E) = (e^2/h)T$ where $T = \mathrm{Tr}[\Gamma_L G^r \Gamma_R G^a]$ is the transmission coefficient. The linewidth function $\Gamma_\alpha(E) = i[\Sigma^r_\alpha - \Sigma^a_\alpha]$ with $\alpha = L, R$ and the Green's functions $G^{r/a}(E)$ are calculated from $G^r = [EI - H_C - \Sigma^r_L - \Sigma^r_R]^{-1}$, where H_C is a Hamiltonian matrix of the central scattering region and I the unity matrix, $\Sigma^r_{L,R}$ are the retarded self-energy due to the device leads. The conductance fluctuation is defined as $\mathrm{rms}(G) \equiv \sqrt{\langle G^2\rangle - \langle G\rangle^2}$, where $\langle\cdots\rangle$ denotes averaging over an ensemble of samples with different disorder configurations having the same Δ value.

[1] C. L. Kane and E. J. Mele, Phys. Rev. Lett. **95**, 146802 (2005).
[2] B. A. Bernevig, T. L. Hughes, and S. C. Zhang, Science **314**, 1757 (2006).
[3] M. Z. Hasan and C. L. Kane, Rev. Mod. Phys. **82**, 3045 (2010); J. E. Moore, Nature (London) **464**, 194 (2010); X. L. Qi and S. C. Zhang, Rev. Mod. Phys. **83**, 1057 (2011); Phys. Today **63**, 33 (2010).
[4] L. Fu and C. L. Kane, Phys. Rev. Lett. **100**, 096407 (2008); **102**, 216403 (2009).
[5] Y. Xia, D. Qian, D. Hsieh, L. Wray, A. Pal, H. Lin, A. Bansil, D. Grauer, Y. S. Hor, R. J. Cava, and M. Z. Hasan, Nat. Phys. **5**, 398 (2009); D. Hsieh, Y. Xia, D. Qian, L. Wray, J. H. Dil, F. Meier, J. Osterwalder, L. Patthey, J. G. Checkelsky, N. P. Ong, A. V. Fedorov, H. Lin, A. Bansil, D. Grauer, Y. S. Hor, R. J. Cava, and M. Z. Hasan, Nature (London) **460**, 1101 (2009); Y. Zhang, K. He, C. Z. Chang, C. L. Song, L. L. Wang, X. Chen, J. F. Jia, Z. Fang, X. Dai, W. Y. Shan, S. Q. Shen, Q. Niu, X. L. Qi, S. C. Zhang, X. C. Ma, and Q. K. Xue, Nat. Phys. **6**, 584 (2010).

[6] W. Dang, H. Peng, H. Li, P. Wang, and Z. F. Liu, Nano Lett. **10**, 2870 (2010); D. Kong *et al.*, *ibid.* **10**, 329 (2010).
[7] J. Li, R. L. Chu, J. K. Jain, and S. Q. Shen, Phys. Rev. Lett. **102**, 136806 (2009).
[8] C. W. Groth, M. Wimmer, A. R. Akhmerov, J. Tworzydlo, and C. W. J. Beenakker, Phys. Rev. Lett. **103**, 196805 (2009).
[9] H.-M. Guo, G. Rosenberg, G. Refael, and M. Franz, Phys. Rev. Lett. **105**, 216601 (2010).
[10] Y. X. Xing, L. Zhang, and J. Wang, Phys. Rev. B **84**, 035110 (2011).
[11] M. Levin and A. Stern, Phys. Rev. Lett. **103**, 196803 (2009).
[12] D. N. Sheng, Z. C. Gu, K. Sun and L. Sheng, Nat. Comm. **2**, 389 (2010).
[13] E. Tang, J. W. Mei, and X. G. Wen, Phys. Rev. Lett. **106**, 236802 (2011).
[14] K. Sun, Z. Gu, H. Katsura, and S. Das Sarma, Phys. Rev. Lett. **106**, 236803 (2011).
[15] T. Neupert, L. Santos, C. Chamon, and C. Mudry, Phys. Rev. Lett. **106**, 236804 (2011).
[16] H. J. Zhang, C. X. Liu, X. L. Qi, X. Dai, Z. Fang, and S. C. Zhang, Nat. Phys. **5**, 438 (2009). Using the parameters taken from this reference and the Hamiltonian Eq. (1), a *bulk* band gap of about 0.50eV is obtained that is crossed by the two linear Dirac bands schematically shown in Fig. 1(c).
[17] We have also examined the robustness of the parameters in Eq. (1) on the formation of type-I helical states (stripe states). If A_1 or B_1 is zero, the states locate only in the x-z plane regardless of energy. If A_2 or D_2 is zero, the states locate only in the x-y plane. B_2 and M are essential: If any one is zero, no topological state is found. D_1 is an irrelevant parameter to the formation of the topological states.
[18] W. Y. Shan, H. Z. Lu, and S. Q. Shen, New J. Phys. **12**, 043048 (2010).
[19] For $L = 20$ and with four orbitals per site, the dimension of the Hamiltonian matrix is 32 000, together with the configurational average over the disorder distribution, the calculation is computationally very demanding. For $L = 20$, there is one subband in the bulk gap with two propagating modes $N = 2$ along the transport direction. For the second and higher subbands to contribute to transport $L = 40$ or larger is required. The largest system we considered is up to $L = 60$ which has five subbands for which the Hilbert space is spanned by 864 000 orbitals and the transport calculation became extremely demanding even for the recursive Green's function method.
[20] C. W. J. Beenakker, Rev. Mod. Phys. **69**, 731 (1997).
[21] To confirm that the quantization plateau, i.e., $\Delta = [0.38, 1.25]$ in Fig. 3, lies in the mesoscopic diffusive regime, we calculated the localization length ξ for this range of Δ. We found $\xi/L = 6 \sim 8$ in this range, i.e., $\xi \gg L$ indicating that the localization physics does not play an important role on the quantized plateau.
[22] D. A. Abanin and L. S. Levitov, Science **317**, 641 (2007).
[23] C. X. Liu, X. L. Qi, H. J. Zhang, X. Dai, Z. Fang, and S. C. Zhang, Phys. Rev. B **82**, 045122 (2010).
[24] J. Chen, H. J. Qin, F. Yang, J. Liu, T. Guan, F. M. Qu, G. H. Zhang, J. R. Shi, X. C. Xie, C. L. Yang, K. H. Wu, Y. Q. Li, and L. Lu, Phys. Rev. Lett. **105**, 176602 (2010).
[25] H.-T. He, G. Wang, T. Zhang, I.-K. Sou, G. K. L. Wong, J.-N. Wang, H.-Z. Lu, S.-Q. Shen, and F.-C. Zhang, Phys. Rev. Lett. **106**, 166805 (2011).
[26] J. R. Williams, L. DiCarlo, and C. M. Marcus, Science **317**, 638 (2007).
[27] C. Mann, D. West, I. Miotkowski, Y. P. Chen, S. Zhang, and C.-K. Shih, Nat. Commun. **4**, 2277 (2013).